Hindawi Publishing Corporation
EURASIP Journal on Wireless Communications and Networking
Volume 2009, Article ID 641292, 9 pages
doi:10.1155/2009/641292

Research Article

Time and Frequency Synchronisation in 4G OFDM Systems

Adrian Langowski

Chair of Wireless Communications, Poznan University of Technology, Polanka 3A, 61-131 Poznan, Poland

Correspondence should be addressed to Adrian Langowski, alangows@et.put.poznan.pl

Received 30 June 2008; Revised 28 October 2008; Accepted 20 December 2008

Recommended by Erchin Serpedin

This paper presents a complete synchronisation scheme of a baseband OFDM receiver for the currently designed 4G mobile communication system. Since the OFDM transmission is vulnerable to time and frequency offsets, accurate estimation of these parameters is one of the most important tasks of the OFDM receiver. In this paper, the design of a single OFDM synchronisation pilot symbol is introduced. The pilot is used for coarse timing offset and fractional frequency offset estimation. However, it can be applied for fine timing synchronisation and integer frequency offset estimation algorithms as well. A new timing metric that improves the performance of the coarse timing synchronisation is presented. Time domain synchronisation is completed after receiving this single OFDM pilot symbol. During the tracking phase, carrier frequency and sampling frequency offsets are tracked and corrected by means of the nondata-aided algorithm developed by the author. The proposed concept was tested by means of computer simulations, where the OFDM signal was transmitted over a multipath Rayleigh fading channel characterised by the WINNER channel models with Doppler shift and additive white Gaussian noise.

1. Introduction

Due to its many advantages, orthogonal frequency division multiplexing (OFDM) was adopted for the European standards of terrestrial stationary and handheld video broadcasting systems (DVB-T, DVB-H) as well as wireless network standards 802.11 and 802.16. It was also chosen as one of the transmission techniques for 3GPP Long-Term Evolution system and WINNER Radio Interface Concept [1], which has recently been proposed for 4G systems. However, the OFDM transmission is sensitive to receiver synchronisation imperfections. The symbol timing synchronisation error may cause *interblock interference* (IBI) and the frequency synchronisation error is one of the sources of *intercarrier interference* (ICI). Thus, synchronisation is a crucial issue in an OFDM receiver design. It depends on the form of the OFDM transmission (whether it is continuous or has a bursty nature). In case of the WINNER MAC superframe structure shown in Figure 1 [2], synchronisation algorithms specific for packet or bursty transmission have to be applied.

Synchronisation is not fully obtained after the acquisition mode since the sampling frequency offset still remains uncompensated. The inaccuracy of the sampling clock frequency causes slow drift of the FFT window giving rise to ICI and subcarrier phase rotation. Both signal distortions, but not their sources, may be removed by a frequency-domain channel equaliser. However, the time shift of the FFT window builds up, and eventually the FFT window shifts beyond the orthogonality window of the OFDM symbol giving rise to IBI. Therefore, the sampling clock synchronisation, performed by a resampling algorithm, should also be implemented in the OFDM receiver.

A number of time and frequency synchronisation algorithms in the OFDM-based systems have already been proposed. The less complex but less accurate algorithms are based on the correlation of identical parts of the OFDM symbol. The correlation between the cyclic prefix and the corresponding end of the OFDM symbol, or between two identical halves of the synchronisation symbol, is applied in [3, 4], respectively. The use of pseudonoise sequence correlation properties was proposed in [5, 6]. Both solutions offer very accurate time and frequency offset estimates; however, the main disadvantage of both of them is their complexity.

The sampling frequency offset estimation has been investigated in many papers too. Since sampling period

offset causes subcarrier phase rotation, some algorithms, like those introduced in [7, 8], estimate the phase change between the subcarriers of the OFDM symbol or between the same subcarriers of succeeding OFDM symbols (see the method described in [9]). A noncoherent solution, that is, without carrier phase estimates, was proposed in [10]. The drawback of that algorithm is its sensitivity to symbol timing synchronisation errors. Like the schemes shown in [7, 8], it requires pilot tones transmitted in every OFDM symbol, as it is done in the DVB-T system. Thus, such algorithms are not suitable for systems with pilot tones separated in time by data symbols, as it can be found in the WINNER system. The algorithm described in [9] is driven by data hard decisions made by the receiver, and it estimates and tracks the residual carrier frequency offset as well. That solution will be compared with the proposed algorithm in Section 7.2.

In this paper, fast and accurate timing and frequency synchronisation algorithms are proposed. The synchronisation is a two-stage process. First, coarse timing and fractional frequency offset synchronisation are performed. After detecting the transmitted signal, the carrier frequency and sampling frequency offsets are tracked during the tracking mode by a low-complex algorithm, which is immune to symbol timing offset estimation errors. The algorithm is designed for OFDM systems with a small pilot overhead, and it applies channel estimates already computed by the channel estimation block.

The paper is organised as follows. In Section 2, the system model is introduced. Section 3 contains the description of the acquisition mode algorithms. In Section 4, timing synchronisation errors are briefly characterised. Sections 5 and 6 contain the description of the decision-directed algorithm and the newly proposed algorithm in which channel transfer function estimates are used. Computer simulation results are presented and discussed in Section 7, and finally, the paper is concluded in Section 8.

2. System Model

The system of interest uses OFDM symbols with $K_U < N$ subcarriers for the data transmission. The remaining $N - K_U$ subcarriers serve as a guard band. The time domain samples are computed using the well-known IFFT formula

$$x_k(n) = \frac{1}{\sqrt{N}} \sum_{m=0}^{K_U-1} X_k(m) e^{j\omega_N mn}, \tag{1}$$

where k is the index of the OFDM symbol, $X_k(m)$ is the frequency domain mth modulated symbol, $\omega_N = 2\pi/N$, and N is the total number of subcarriers.

Let us assume that the OFDM signal model developed within the WINNER project [1]. The OFDM symbol consists of $N = 2048$ subcarriers out of which $K_U = 1664$ are used for transmission of user data and pilots. The user data are transmitted in packets called chunks. Every chunk consists of 8 subcarriers and lasts for 12 OFDM symbols. Within each chunk, there are 4 pilot tones spaced by $D_t = 10$ OFDM symbols and by $D_f = 4$ subcarriers [11]. Their pattern is shown in Figure 2. Generated OFDM symbols are grouped into packets and transmitted over a Rayleigh fading multipath channel for which the impulse response is

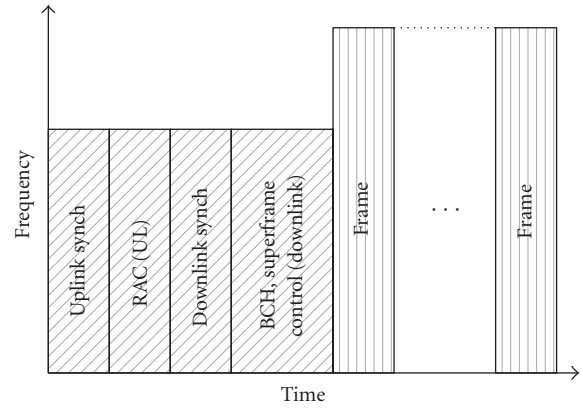

Figure 1: WINNER MAC superframe structure.

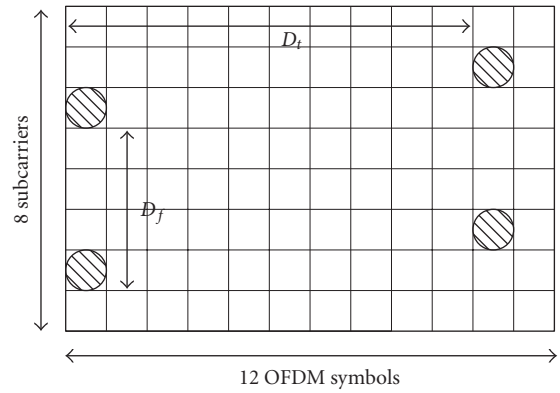

Figure 2: Pilot tones pattern within the chunk.

$$h(\tau, t) = \sum_{l=0}^{L-1} h_l(t)\delta(\tau - \tau_l), \tag{2}$$

where $h_l(t)$ is the complex channel coefficient of the lth path, τ_l is the delay of the lth path, and L is the number of channel paths.

3. Data-Aided Correlation Scheme

3.1. Coarse Timing Synchronisation. Downlink timing synchronisation should be performed during the *Downlink Synch* slot of the WINNER MAC superframe [2]. The first OFDM symbol of the *Downlink Synch* is called the *T-Pilot* and is dedicated to the synchronisation process. Two synchronisation symbol designs have been considered as possible *T-Pilots*. Their time-domain structures are illustrated in Figure 3. The first one is used together with the original Schmidl and Cox algorithm [4], and the latter one is used with a modified version of the Schmidl and Cox algorithm proposed by the author. In order to generate OFDM symbols consisting of 2 and 8 identical elements, BPSK representation of the Gold sequence is transmitted on every second and eighth subcarrier of the OFDM symbol, respectively. If the

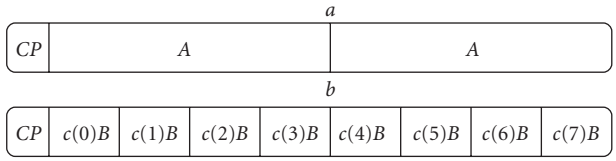

Figure 3: Time-domain structures of the considered synchronisation symbols.

Schmidl and Cox algorithm is applied together with the second candidate synchronisation symbol, the time metric plateau occurs after the first subsymbol. The problem is solved by multiplying the already generated time-domain OFDM symbol by the sign coefficients $c(i)$ $(i = 0, \ldots, 7)$ that are defined as

$$\begin{aligned}\mathbf{c} &= [c(0), c(1), c(2), c(3), c(4), c(5), c(6), c(7)] \\ &= [-1, 1, 1, 1, 1, 1, 1, 1].\end{aligned} \tag{3}$$

In order to perform the coarse timing synchronisation, both subsymbols of the first candidate preamble and the first four subsymbols of the latter candidate preamble are used. The remaining subsymbols of the second candidate preamble are used for fractional frequency offset estimation. In order to obtain the best of the 8-element candidate preamble, the new time metric is defined as

$$P(n) = \frac{\left|(1/3)\sum_{i=0}^{2} c(i) \sum_{l=0}^{L-1} y_{\text{late}}(n,l,i)\, y^{\star}_{\text{early}}(n,l,i)\right|^2}{\left(\sum_{l=0}^{L-1} |y(n-l-L)|^2\right)^2}, \tag{4}$$

where $y_{\text{late}}(n,l,i) = y(n-l-(3-i)L)$, $y_{\text{early}}(n,l,i) = y(n-l-(2-i)L)$, and $L = N/8$. In the above formula, the numerator is an averaged value of three cross-correlation samples computed between four consecutive sample blocks of length L each. Thus, the quality of the time metric is improved due to noise averaging. Time metric (4) is compared with an appropriately selected detection threshold Γ, and the middle of the OFDM symbol, that is, the maximum value of the time metric, is found among all time metrics greater than the detection threshold. Thus, the beginning of the next OFDM symbol is estimated with the following formula:

$$\hat{\theta} = \arg \max_{n}(P(n)) + \frac{N}{2}, \quad \text{for } P(n) > \Gamma. \tag{5}$$

Detection of the maximum value of (4) ends the coarse timing synchronisation stage. However, fractional frequency estimation needs yet to be performed.

3.2. Fractional Frequency Estimation. The process of frequency synchronisation consists of two stages: frequency offset estimation and correction. Having a preamble of the form shown in Figure 3 at the beginning of each superframe, we are able to estimate the frequency offset using the same procedure as in timing offset estimation. This time, the argument of the correlation between two subsequent pilot symbols determines the frequency offset, that is,

$$\begin{aligned}\gamma(n) &= \sum_{i=n}^{n+L-1} y(i-L)\, y^{\star}(i), \\ \delta\hat{f} &= \frac{1}{2\pi L} \arg\left(\gamma(\hat{\theta})\right),\end{aligned} \tag{6}$$

where $\hat{\theta}$ is the estimated symbol timing. Such an algorithm is able to estimate only a fractional part of the frequency offset, whereas its integer part $l\Delta f$, in terms of the multiples of the currently used subcarrier distance Δf, must be estimated in another way. The distance between the used subcarriers in the pilot subsymbols A is equal to $8\Delta f$ (assuming every subcarrier of every pilot symbol is used), so $\pm 4\Delta f$ is the maximum frequency offset which can be estimated. It can be observed that there are a number of available frequency offset estimates due to repetitive nature of the synchronisation symbol. The correct estimates are computed within the window W starting from the end of the third subsymbol A and ending at the end of the last subsymbol. This implies that the frequency offset estimation quality can be improved by averaging the estimates computed during the window W, that is,

$$\hat{\delta} f_W = \frac{1}{W 2\pi L} \sum_{i=N_G/2}^{W+N_G} \arg\left(\gamma(\hat{\theta} - i)\right), \quad \text{for } W = 1, \ldots, 4L, \tag{7}$$

where N_G is the cyclic prefix length. The use of the offset equal to $N_G/2$ in averaging aims to compensate the influence of the symbol timing estimation error on the computed frequency offset.

4. Postacquisition Synchronisation Errors

Assuming that the timing synchronisation was successful enough to find the OFDM symbol start within the IBI-free region, two kinds of frequency offsets remain after the acquisition mode, that is, sampling period offset (SPO) and residual carrier frequency offset (CFO). Denote $\epsilon = (T_s' - T_s)/T_s$ as the normalised SPO and $\delta f_N = \delta f/\Delta f$ as the normalised frequency offset, where T_s', T_s, δf, and Δf are real sampling period, the ideal sampling period, carrier frequency offset, and subcarrier distance, respectively. The data symbol received on the mth subcarrier of the kth OFDM symbol is described by [9, 12, 13]

$$\begin{aligned}Y_k(m) = \alpha(\theta(m)) X_k(m) H_k(m) e^{j\pi\theta(m)(N-1)/N} \\ \times e^{j2\pi\theta(m)(N_G+kM)/N} + ICI_k(m) + N_k(m),\end{aligned} \tag{8}$$

where $\theta(m) = \delta f_N(1+\epsilon) + m\epsilon \approx \delta f_N + m\epsilon$, $M = N + N_G$, $\alpha(\theta(m))$ is an attenuation caused by both offsets, and $N_k(m)$ is the Gaussian noise sample.

The sampling period offset affects the OFDM signal in two ways. First, it rotates data symbols. Second, since accumulated sampling period offset is not constant during

the OFDM symbol but increases from sample to sample, it disturbs the orthogonality of the subcarriers giving rise to intercarrier interference. However, for small offsets the second phenomenon and the attenuation are negligible, and they will not be considered in this work.

5. Decision-Directed Algorithm

Decision-directed (DD) estimation of the sampling period offset and carrier frequency offset was proposed in [9] and is presented here as a reference to our method. First, the phase-difference-dependent signal $\lambda_k^{\mathrm{DD}}(m)$ for each subcarrier is computed

$$\lambda_k^{\mathrm{DD}}(m) = \frac{Y_k(m)Y_{k-1}^{\star}(m)}{\widetilde{D}_k(m)\widetilde{D}_{k-1}^{\star}(m)}, \tag{9}$$

where $\widetilde{D}_k(m)$ is the hard data decision, and $(\cdot)^{\star}$ denotes the complex conjugate. The arguments of the above signals are then used for CFO and SPO estimation:

$$\begin{aligned} \delta\widetilde{f}_{N_k} &= \frac{\rho}{2\pi}\frac{\varphi_{k,1}+\varphi_{k,2}}{2}, \\ \widetilde{\epsilon}_k &= \frac{\rho}{2\pi}\frac{\varphi_{k,2}-\varphi_{k,1}}{(K_U/2)+1}, \end{aligned} \tag{10}$$

where

$$\varphi_{k,1} = \arg\left(\sum_{i\in\mathbb{C}_1}\lambda_k^{\mathrm{DD}}(i)\right), \qquad \varphi_{k,2} = \arg\left(\sum_{i\in\mathbb{C}_2}\lambda_k^{\mathrm{DD}}(i)\right), \tag{11}$$

and $\mathbb{C}_1 = \langle -K_U/2, -1\rangle$ and $\mathbb{C}_2 = \langle 1, K_U/2\rangle$ are the sets of indices of the first and the second half of the OFDM signal band, respectively, and $\rho = N/M$. The one-shot estimates are filtered using the first-order tracking loop filter:

$$\begin{aligned} \delta\widehat{f}_{N_k} &= \delta\widehat{f}_{N_{k-1}} + \gamma_f\delta\widetilde{f}_{N_k}, \\ \widehat{\epsilon}_k &= \widehat{\epsilon}_{k-1} + \gamma_\epsilon\widetilde{\epsilon}_k, \end{aligned} \tag{12}$$

where γ_f and γ_e are CFO and SPO loop filters coefficients, respectively. The sampling period offset estimate controls the *interpolator/decimator* block that corrects the offset. The carrier frequency offset is used for correcting the phase of the time samples of the received OFDM signal. The drawback of this algorithm is that the CFO estimate does not take into consideration the influence of SPO that can be significant during the initialisation of the algorithm.

6. Proposed Algorithm

6.1. CFO and SPO Estimation. The phase rotation of the subcarrier is easily detectable by the channel estimator and is estimated jointly with the channel transfer function. Thus, the generalised CTF takes the form

$$H_k'(m) = H_k(m)e^{j\pi\theta(m)(N-1)/N}e^{j2\pi\theta(m)(N_G+kM)/N}. \tag{13}$$

The author proposes to apply the knowledge obtained by the channel estimator for sampling period offset correction. The phase-difference-dependent variable $\lambda_k(m)$ is defined as follows:

$$\lambda_k(m) = \widetilde{H}_k'(m)\widetilde{H}_{k-1}'^{\star}(m), \tag{14}$$

where $\widetilde{H}_k(m)$ is the CTF estimate of the mth channel. Instead of using an *interpolator/decimator* block, the proposed scheme corrects the subcarrier phases. This implies that the intercarrier interference remains unchanged, however, the receiver is simpler and cheaper. Another consequence of this solution is that the FFT window drift during one OFDM symbol is estimated instead of the exact sampling period offset. After substituting (13) into (14) and modifying the intermediate result, the phase-difference-dependent $\lambda_k(m)$, assuming $H_{k+1}(m) \approx H_k(m)$, is defined as

$$\lambda_k(m) = \left|\widetilde{H}_k'(m)\right|^2 e^{j2\pi(\delta f_N+\epsilon m)/\rho}. \tag{15}$$

Then, the one-shot sampling frequency offset estimate is given by

$$\widetilde{\epsilon}_{M,k} = \frac{N}{2\pi}\frac{\varphi_{\epsilon,k}}{(K_U/2)+1}, \tag{16}$$

where

$$\begin{aligned} \varphi_{\epsilon,k} &= \arg\left(\sum_{i\in\mathbb{C}_1}\lambda_k\left(i+\frac{K_U}{2}+1\right)\lambda_k^{\star}(i)\right) \\ &\approx \frac{2\pi}{\rho}\epsilon\left(\frac{K_U}{2}+1\right), \end{aligned} \tag{17}$$

and $\mathbb{C}_1$ is the set of indices of the pilot subcarriers in the first half of the OFDM signal band. The approximation in (17) becomes exact if the channel transfer function estimates $\widetilde{H}_k'(m)$ $(m = 1,\ldots,N)$ are ideal and there is no additive noise. The algorithm computes the FFT window offset caused by the sampling period error accumulated during one OFDM symbol instead of estimating the exact sampling period error itself. In order to estimate the carrier frequency offset, the phase $\varphi_{f,k}$ is computed first:

$$\begin{aligned} \varphi_{f,k} &= \arg\left(\sum_{i\in\mathbb{C}_1}\lambda_k\left(i+\frac{K_U}{2}+1\right)\lambda_k(i)\right) \\ &\approx \frac{2\pi}{\rho}2\delta f_N + \frac{2\pi}{\rho}\epsilon\left(\frac{K_U}{2}+1\right) + N_k, \end{aligned} \tag{18}$$

where

$$N_k = \arg\sum_{i\in\mathbb{I}_1}e^{j(2\pi/\rho)2\epsilon i}\left|\widetilde{H}_k'\left(i+\frac{K_U}{2}+1\right)\right|^2\left|\widetilde{H}_k'(i)\right|^2 \tag{19}$$

can be interpreted as a phase noise caused by the sampling frequency offset. It can be seen that the second component in (18) is equal to the phase given by (17) and in this case is undesired. Thus, the one-shot CFO estimate is given by

$$\delta\widetilde{f}_{N,k} = \frac{\rho}{2\pi}\frac{\varphi_{f,k}-\varphi_{\epsilon,k}}{2}. \tag{20}$$

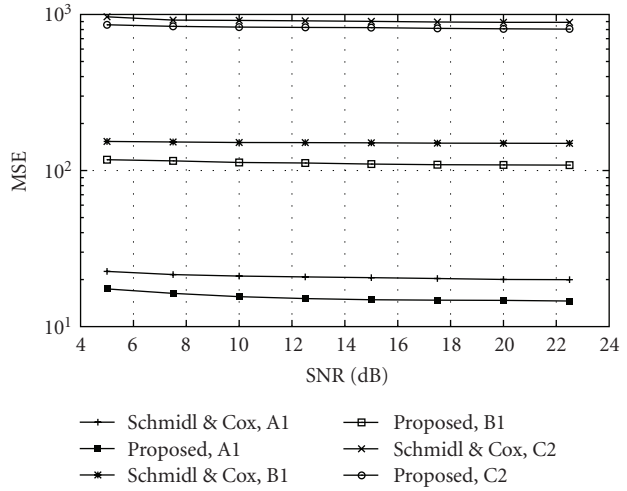

Figure 4: Timing synchronisation MSE of Schmidl and Cox algorithm and the proposed algorithm for A1, B1, and C2 channels.

6.2. DPLL. Both sampling frequency offset estimate $\widetilde{\epsilon}_{M,k}$ and carrier frequency offset estimate $\delta\widetilde{f}_{N,k}$ are fed to two second-order *digital phase-locked loop* (DPLL) filters whose block diagram is presented in Figure 5. Coefficients μ_1 and μ_2 are the proportional and integral coefficients, respectively. The transfer function of the DPLL is [14]

$$\begin{aligned} H(z) &= \frac{\mu_2(z-1)+\mu_1}{(z-1)^2+\mu_2(z-1)+\mu_1} \\ &= \frac{2\zeta\omega_n(z-1)+\omega_n^2}{(z-1)^2+2\zeta\omega_n(z-1)+\omega_n^2}, \end{aligned} \tag{21}$$

where $\mu_2 = 2\zeta\omega_n T_s$, $\mu_1 = \mu_2^2/4\zeta^2$, $\omega_n = 2\pi f_n$, T_s is the sampling period, ζ is the damping factor, and f_n is the natural frequency of the loop. In order to guarantee the stability of the loop, the damping factor ζ and the natural frequency f_n must satisfy the following relationship [15]:

$$\begin{gathered} \zeta > 1, \\ 0 < \omega_n < 2, \\ \zeta\omega_n < \left(\frac{\omega_n^2}{4}\right) + 1, \end{gathered} \quad \text{or} \quad \begin{gathered} \zeta \le 1, \\ 0 < \omega_n < 2\zeta. \end{gathered} \tag{22}$$

From the sampling frequency offset loop output $\widehat{\epsilon}_{M,k}$ the integer $\widehat{\epsilon}_{\text{int}}$ and fractional part $\widehat{\epsilon}_{\text{fra}}$ of the accumulated sampling period error are extracted. The integer part is used for correcting the FFT window while the fractional part is used for correcting the subcarriers phase.

6.3. Channel Estimation. As we know, in the proposed CFO and SPO estimation algorithms, estimation of the channel transfer function is needed. The channel transfer function estimate may be computed using any algorithm that gives reliable estimates. In our design, the *Zero Force* (ZF) channel

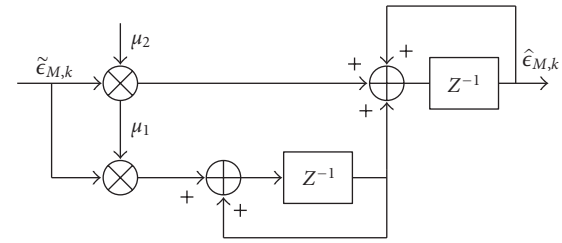

Figure 5: Second-order digital phase-locked loop filter diagram.

estimator was applied to obtain the initial channel estimate [16]:

$$\widetilde{H}_1(m) = \frac{\widetilde{D}_i^{\star}(m)Y_1(m)}{|\widetilde{D}_i(m)|^2}. \tag{23}$$

The symbol $\widetilde{D}_i(m)$ is the hard decision made by the demodulator; however, when the first OFDM symbol of the superframe is received, the symbol represents the pilot symbol known to the receiver. After receiving the first OFDM symbol, the estimator switches to the tracking mode. The channel estimates are refined and tracked according to the gradient algorithm, which minimises the *mean square error* (MSE) [17]

$$\widetilde{H}_{k+1}(m) = \widetilde{H}_k(m) + \alpha_H\left(Y_k(m) - \widetilde{H}_k(m)\widetilde{D}_k(m)\right)\widetilde{D}_k^{\star}(m), \tag{24}$$

where α_H is the coefficient dependent on transmitted symbols power and is constant during the transmission. The channel coefficients are updated every received OFDM symbol. The author would like to stress that the channel estimation algorithm is not an integral part of the carrier frequency and sampling frequency offset estimation algorithm and other channel estimation algorithms can be applied as well.

7. Simulation Results

The proposed synchronisation scheme was tested for the WINNER system parameters presented in Table 1. The Rayleigh fading channels were simulated using 20-path NLOS channel models, denoted as A1, B1, and C2, with root-mean square delay spreads τ_{RMS} equal to 24.15, 94.73, and 310 nanoseconds, respectively. These models were developed within the WINNER project for indoor/small office, typical urban (TU) microcellular and macrocellular environments [18]. The simulation results were obtained using 10 000 channel realisations for each SNR value.

7.1. Acquisition. As a first test, the comparison of the accuracy of the timing synchronisation using the proposed time metric with the 8-element synchronisation symbol with respect to the accuracy of the Schmidl and Cox synchronisation algorithm using 2-element synchronisation symbol was performed. The results are presented in Figure 4. The performance of the new metric is slightly better than the

Table 1: WINNER signal parameters.

	Base Coverage Urban	Microcellular	Indoor
Carrier frequency	3.95 GHz DL	3.95 GHz	3.95 GHz
Signal bandwidth	2×45 MHz	89.84 GHz	89.84 GHz
Subcarrier distance	39062.5 Hz	48828.125 Hz	48828.125 Hz
Used subcarriers	1152	1840	1840
IFFT size N	2048	2048	2048
Prefix length N_G	256	200	200
Channel models	C2	B1	A1
Max velocity	19.44 m/s	19.44 m/s	1.39 m/s
Packet langth	192	192	192

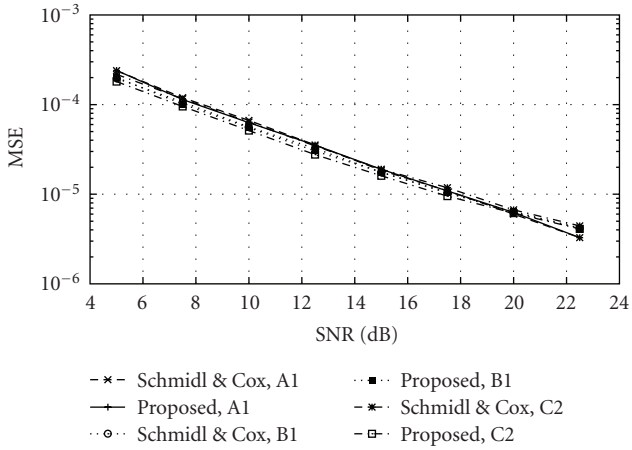

Figure 6: Frequency synchronisation MSE of Schmidl and Cox algorithm and the proposed algorithm for A1, B1, and C2 channels.

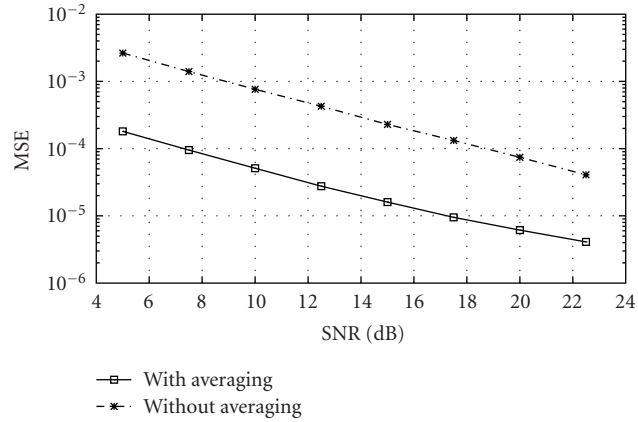

Figure 7: Frequency synchronisation MSE with and without averaging of the frequency offset estimate.

performance of the latter one in all three scenarios. However, as opposed to Schmidl and Cox method, the proposed coarse timing synchronisation is already finished at the beginning of the second half of the synchronisation symbol.

Results of both fractional frequency offset estimation algorithms, obtained for three different channels, are presented in Figure 6. The algorithms performance was tested for the frequency offsets close to the maximum frequency offsets that the algorithms are able to estimate, that is, $0.99\Delta f$ for Schmidl and Cox algorithm and $3.99\Delta f$ for the proposed solution. Although the correlation length in the proposed algorithm is four times shorter than in the Schmidl and Cox algorithm, the accuracy of both solutions is almost the same, regardless of the transmission scenario. Similar performance between the proposed solution and the reference algorithm is achieved as a result of the averaging of the estimates computed during the reception of the synchronisation symbol. The comparison of the accuracy of the algorithm with and without averaging is illustrated in Figure 7. The averaging decreases the MSE approximately by a factor of 10 for all SNR values.

If the frequency offset is larger than four times subcarrier distance, an integer frequency offset estimation algorithm, like the one described in [19] or [20], is required.

7.2. Tracking. During the tracking mode, randomly generated user data and pilots were mapped onto a QPSK constellation. Loops' parameters used by both algorithms during simulations are shown in Table 2.

The algorithms for the carrier frequency and sampling frequency offsets estimation and tracking were tested for frequency offsets of $\delta f = 0.01$ and $\delta f = 0.05$ and the sampling frequency offsets of $\delta T_s = 5$ ppm and 30 ppm. The second frequency offset was chosen to be larger than the maximum frequency offset estimation error of the frequency synchronisation algorithm. The results of SPO estimation are illustrated in Figures 8, 9, and 10 for A1, B1, and C2 scenarios, respectively. The mean square error of the estimated SPO is the same in the whole used SNR range, except for small signal power in the C2 scenario. The influence of the channel estimator inaccuracy on the proposed algorithm performance is visible when compared with the results achieved for the AWGN channel only. The mean square error floor occurs for large SNR values due to the Rayleigh fading channel and its estimation.

The same error floor behaviour can be observed during the estimation of the carrier frequency offset (see Figures 11, 12, and 13). In A1 and C2 scenarios, the algorithm estimates small δf more accurately than the larger offsets for small

Table 2: DPLL loops parameters.

Channel model	Algorithm	SFO DPLL		CFO DPLL	
		ζ	ω_n	ζ	ω_n
A1	DD	0.20	0.20	0.40	0.50
	proposed	0.30	0.20	0.40	0.50
B1	DD	0.30	0.20	0.40	0.50
	proposed	0.35	0.20	0.50	0.30
C2	DD	0.23	0.44	0.40	0.50
	proposed	0.23	0.44	0.30	0.50

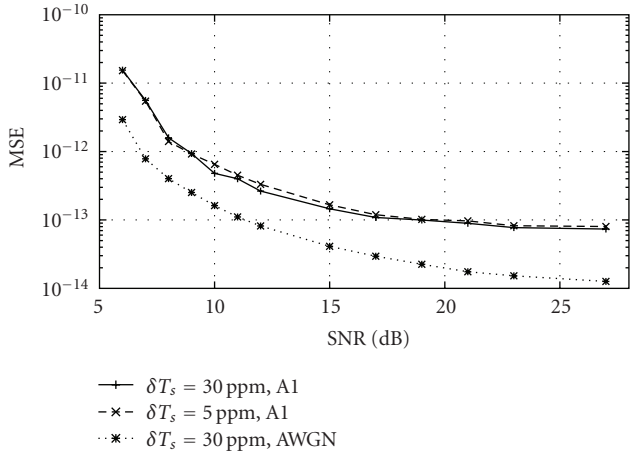

Figure 8: The mean square error of the estimated SPO in A1 channel.

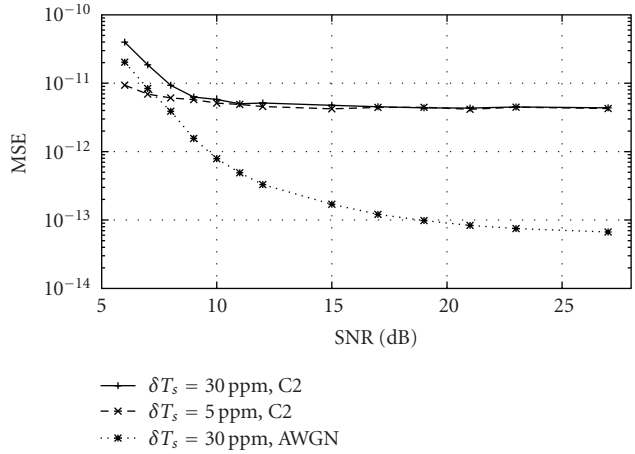

Figure 10: The mean square error of the estimated SPO in C2 channel.

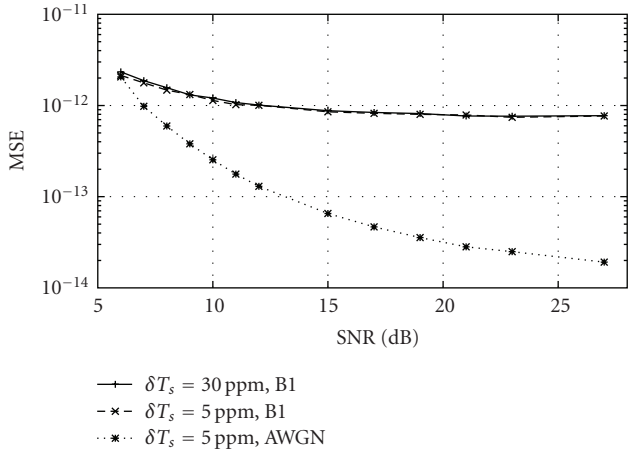

Figure 9: The mean square error of the estimated SPO in B1 channel.

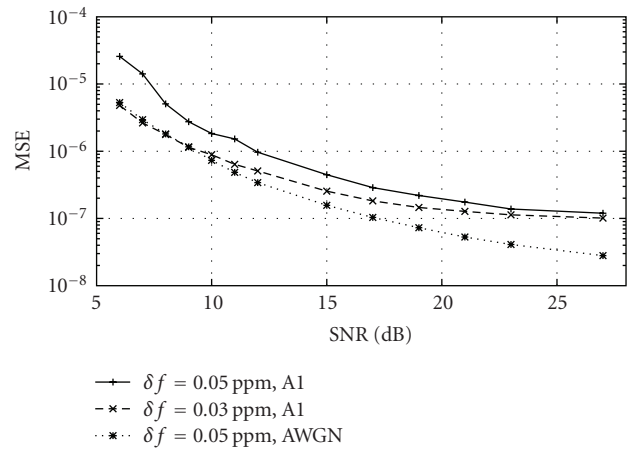

Figure 11: The mean square error of the estimated CFO in A1 channel.

SNRs. However, again an MSE floor occurs for large SNR values.

The performance of the proposed carrier frequency offset and sampling period offset estimation algorithm was tested for small and large velocities of the terminal with respect to its maximum value. The simulation results, obtained for SNR=30 dB, $\delta T_s = 30$ pps, and $\delta f = 0.05$, are presented in Figure 14 for SPO estimation and in Figure 15 for CFO estimation. The mean square error of the offset estimation degrades rapidly with the low but increasing velocity of the terminal. The degradation slows down for velocities larger than 10 m/s. On average, an increase of the velocity by 10 m/s in B1 and C2 scenarios increases the MSE of the estimated SPO and CFO approximately by a factor of 1.5. An increase of the velocity by 1 m/s in A1 scenario increases the MSE of the estimated SPO and CFO by a factor of 1.2.

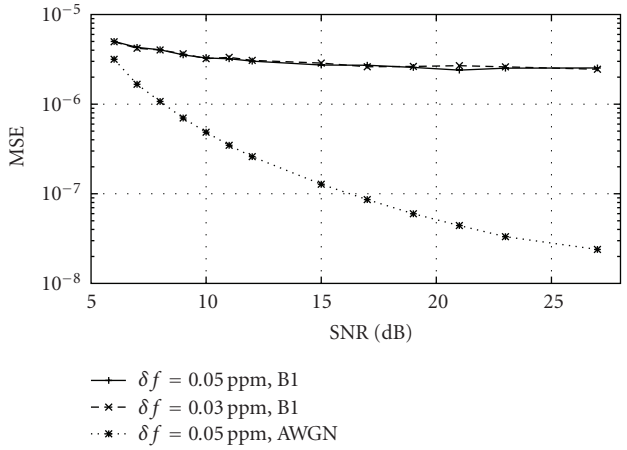

Figure 12: The mean square error of the estimated CFO in B1 channel.

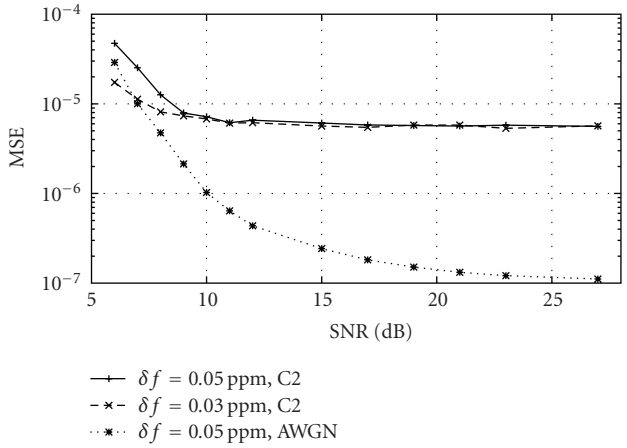

Figure 13: The mean square error of the estimated CFO in C2 channel.

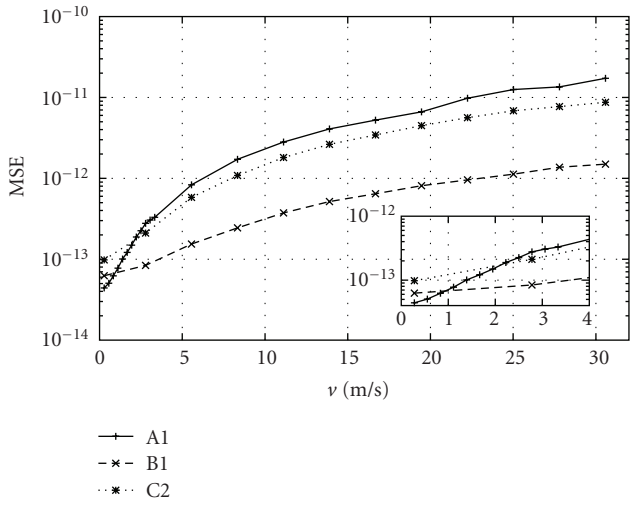

Figure 14: The mean square error of the estimated SPO for different values of mobile velocity.

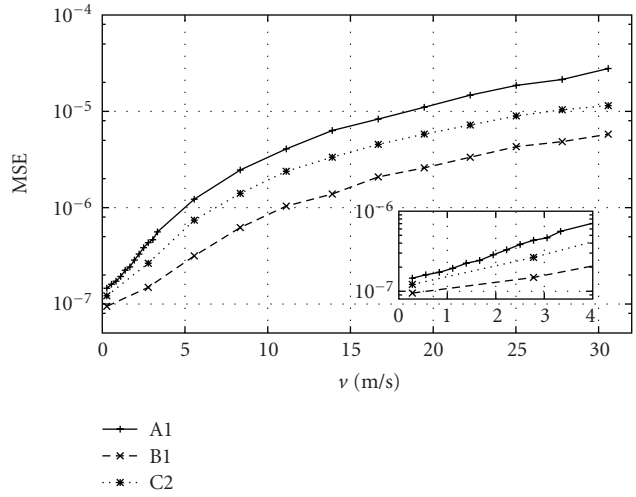

Figure 15: The mean square error of the estimated CFO for different values of mobile velocity.

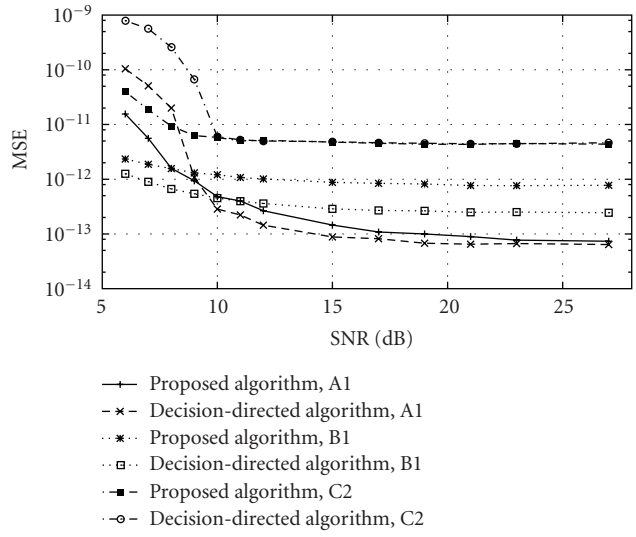

Figure 16: The mean square error of the estimated SFO for $\delta T_s = 30$ ppm.

Finally, both algorithms, that is, the proposed and decision-directed algorithms, are compared in all scenarios for a sampling period offset of $\delta T_s = 30$ ppm and a CFO of $\delta f = 0.05$. However, as with to the proposed solution, carrier frequency and sampling period offsets estimated by the DD algorithm were filtered using the second-order DPLL. Both solutions used the same sets of subcarrier indices $\mathbb{C}_1$ and $\mathbb{C}_2$. The results plotted in Figures 16 and 17 indicate that for low SNR values the proposed algorithm copes better with severe channel conditions than the decision-directed one, especially in A1 and C2 scenarios. Poor performance of the DD algorithm is related to the increase of the channel estimate phase error due to the hard decisions made by the data demodulator and propagation of the phase error to the phase-difference-dependent signal (9). Because the proposed solution does not use hard decisions, the phase errors of

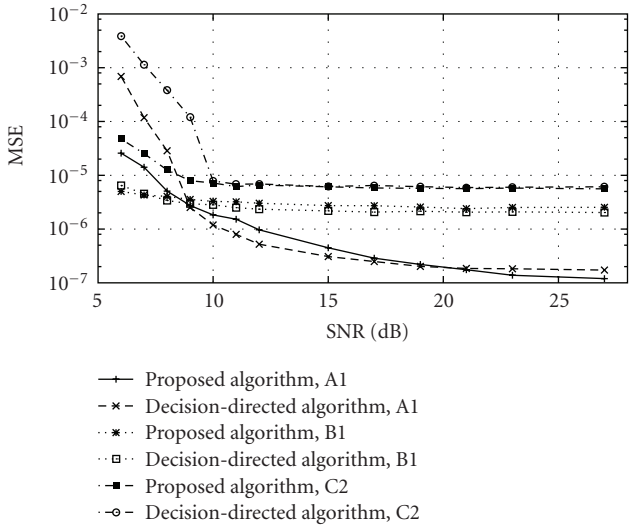

Figure 17: The mean square error of the estimated CFO for $\delta f = 0.05$.

the erroneous channel estimates are not amplified, and their influence on the overall algorithm performance is smaller than in the DD algorithm.

8. Conclusions

In this paper, link-level synchronisation algorithms designed for the OFDM-based proposal for 4G system developed in the WINNER project have been introduced. A new time metric and pilot symbol design for coarse timing synchronisation, as well as new carrier and sampling frequency offset estimation algorithms, were proposed. The algorithms were tested in three different transmission scenarios. Simulation results showed that on the basis of only one OFDM symbol, the algorithms, at the cost of moderate complexity, gave accurate time and frequency offset estimates. The carrier and sampling frequency offset estimation and tracking algorithm, based on the channel estimates, is suitable for transmission systems with low pilot overhead. Simulation results showed that for low SNR, the proposed algorithm works better than the decision-directed solution.

References

[1] "D2.10: Final report on identified RI key technologies, system concept, and their assessment," Tech. Rep. IST-2003-507581, Information Society Technologies, Yerevan, Armenia, December 2005.

[2] M. Abaii, G. Auer, Y. Cho, et al., "D6.13.7 Test Scenarios and Calibration Cases Issue 2," Tech. Rep. IST-4-027756 WINNER II, Information Society Technologies, Yerevan, Armenia, December 2006.

[3] J.-J. van de Beek, M. Sandell, and P. O. Börjesson, "ML estimation of time and frequency offset in OFDM systems," *IEEE Transactions on Signal Processing*, vol. 45, no. 7, pp. 1800–1805, 1997.

[4] T. M. Schmidl and D. C. Cox, "Robust frequency and timing synchronization for OFDM," *IEEE Transactions on Communications*, vol. 45, no. 12, pp. 1613–1621, 1997.

[5] F. Tufvesson, O. Edfors, and M. Faulkner, "Time and frequency synchronization for OFDM using PN-sequence preambles," in *Proceedings of the 50th IEEE Vehicular Technology Conference (VTC '99)*, vol. 4, pp. 2203–2207, Amsterdam, The Netherlands, September 1999.

[6] C. Yan, J. Fang, Y. Tang, S. Li, and Y. Li, "OFDM synchronization using PN sequence and performance," in *Proceedings of the 14th IEEE International Symposium on Personal, Indoor and Mobile Radio Communications (PIMRC '03)*, vol. 1, pp. 936–939, Beijing, China, September 2003.

[7] D. K. Kim, S. H. Do, H. B. Cho, H. J. Chol, and K. B. Kim, "A new joint algorithm of symbol timing recovery and sampling clock adjustment for OFDM systems," *IEEE Transactions on Consumer Electronics*, vol. 44, no. 3, pp. 1142–1149, 1998.

[8] S. A. Fechtel, "OFDM carrier and sampling frequency synchronization and its performance on stationary and mobile channels," *IEEE Transactions on Consumer Electronics*, vol. 46, no. 3, pp. 438–441, 2000.

[9] K. Shi, E. Serpedin, and P. Ciblat, "Decision-directed fine synchronization in OFDM systems," *IEEE Transactions on Communications*, vol. 53, no. 3, pp. 408–412, 2005.

[10] B. Yang, K. B. Letaief, R. S. Cheng, and Z. Cao, "Timing recovery for OFDM transmission," *IEEE Journal on Selected Areas in Communications*, vol. 18, no. 11, pp. 2278–2291, 2000.

[11] D. Aronsson, G. Auer, S. Bittner, et al., "Link level procedures for the WINNER System," Tech. Rep. IST-4-027756 WINNER II, Information Society Technologies, Yerevan, Armenia, November 2007.

[12] P. H. Moose, "Technique for orthogonal frequency division multiplexing frequency offset correction," *IEEE Transactions on Communications*, vol. 42, no. 10, pp. 2908–2914, 1994.

[13] M. Luise and R. Reggiannini, "Carrier frequency acquisition and tracking for OFDM systems," *IEEE Transactions on Communications*, vol. 44, no. 11, pp. 1590–1598, 1996.

[14] F. M. Gardner, *Phaselock Techniques*, John Wiley & Sons, New York, NY, USA, 2005.

[15] Z.-W. Zheng, Z.-X. Yang, C.-Y. Pan, and Y.-S. Zhu, "Novel synchronization for TDS-OFDM-based digital television terrestrial broadcast systems," *IEEE Transactions on Broadcasting*, vol. 50, no. 2, pp. 148–153, 2004.

[16] J. Proakis, *Digital Communications*, McGraw-Hill, New York, NY, USA, 4th edition, 2001.

[17] A. Langowski, A. Piatyszek, Z. Długaszewski, and K. Wesołowski, "VHDL realisation of the channel estimator and the equaliser in the OFDM receiver," in *Proceedings of the 10th National Symposium of Radio Science (URSI '02)*, pp. 129–134, Poznan, Poland, March 2002.

[18] "D5.4 Final Report on Link Level and System Level Channel Models," Tech. Rep. IST-2003-507581 WINNER, Information Society Technologies, Yerevan, Armenia, September 2005.

[19] K. Bang, N. Cho, J. Cho, et al., "A coarse frequency offset estimation in an OFDM system using the concept of the coherence phase bandwidth," *IEEE Transactions on Communications*, vol. 49, no. 8, pp. 1320–1324, 2001.

[20] Z. Długaszewski and K. Wesołowski, "Simple coarse frequency offset estimation schemes for OFDM burst transmission," in *Proceedings of the 13th IEEE International Symposium on Personal, Indoor and Mobile Radio Communications (PIMRC '02)*, vol. 2, pp. 567–571, Lisbon, Portugal, September 2002.